Highlights of Spanish Astrophysics XII, Proceedings of the XVI Scientific Meeting of the Spanish Astronomical Society held on July 15 - 19, 2024, in Granada, Spain. M. Manteiga, F. González Galindo, A. Labiano Ortega, M. Martínez González, N. Rea, M. Romero Gómez, A. Ulla Miguel, G. Yepes, C. Rodríguez López, A. Gómez García and C. Dafonte (eds.), 2025

Probing Dark Matter in the Intracluster Medium with Microlensing

Fian, C.[1,2], Muñoz, J. A.[1,2], Forés-Toribio, R.[1,2], Mediavilla, E.[3,4] and Jiménez-Vicente, J.[5,6]

[1] Departamento de Astronomía y Astrofísica, Universidad de Valencia, E-46100 Burjassot, Valencia, Spain
[2] Observatorio Astronómico, Universidad de Valencia, E-46980 Paterna, Valencia, Spain
[3] Instituto de Astrofísica de Canarias, Vía Láctea S/N, La Laguna 38200, Tenerife, Spain
[4] Departamento de Astrofísica, Universidad de la Laguna, La Laguna 38200, Tenerife, Spain
[5] Departamento de Física Teórica y del Cosmos, Universidad de Granada, Campus de Fuentenueva, 18071 Granada, Spain
[6] Instituto Carlos I de Física Teórica y Computacional, Universidad de Granada, 18071 Granada, Spain

Abstract

Galaxy clusters, the largest gravitationally-bound structures in the Universe, primarily consist of dark matter, offering a unique opportunity for investigating its distribution and behavior. Our study involves an examination of the stellar-to-smooth dark matter mass fraction in the galaxy cluster lensing the quasar SDSS J1326+4806, while concurrently estimating the size of the quasar's broad-line emitting region through microlensing observations. Utilizing GTC spectra, we are assessing the impact of microlensing on the wings of the C IV high-ionization line. Our Bayesian analysis has revealed that the smooth dark matter fraction near image A is $\sim 88\%$, and the estimated half-light radius for the C IV emitting region is $R_{1/2} = 8.1 \pm 4.3$ light-days.

1 Introduction

The amount and spatial distribution of dark matter relative to stars is a fundamental probe of galaxy cluster formation and evolution. However, accurately measuring this dark matter fraction presents a significant challenge. Microlensing of the images of gravitationally lensed quasars provides a direct means of measuring the dark matter fraction at the location of the lensed images. The microlensing phenomenon arises due to mass "granularities" created by stars and their remnants, which induce time-dependent flux variations in the lensed quasar images (see the review by [22]). Particularly when stars constitute only a minor fraction of the surface mass density, microlensing becomes highly sensitive to the relative proportions of stellar and dark matter in the vicinity of the quasar images (e.g., [20]). Furthermore, quasar size estimates also depend on the fraction of mass in compact microlenses. Consequently, microlensing allows us to estimate the local fraction of mass in stars versus dark matter ([16, 13]), and the size of quasar emission regions ([1, 2]). In this study, we perform a joint analysis of both the dark matter mass fraction and the C IV emitting region size.

The structure of this paper is as follows. Section 2 describes the observational data and outlines our data analysis approach. Section 3 details the microlensing simulations and discusses the application of Bayesian methods to infer the C IV emitting region size and the fraction of compact versus dark matter. In Section 4, we present and discuss our findings. Finally, Section 5 summarizes the key results and outlines our main conclusions.

2 Observations and Data Analysis

This work is based on observations conducted using the 10.4 m Gran Telescopio Canarias (GTC) at the Roque de los Muchachos Observatory in La Palma, Spain, under proposal ID GTC31-24A (PI: Carina Fian). We performed OSIRIS long-slit spectroscopy of SDSS J1326+4806, a quasar at redshift $z = 2.08$, which was discovered by [21]. The quasar appears as two images with a $21''.06$ separation due to gravitational lensing by a massive galaxy cluster. The observations took place on April 3^{rd} 2024 using the R1000B grating, covering the full optical range from 3630 Å to 7000 Å with a spectral sampling of 2.1 Å pix^{-1}. We took a total of nine exposures, each lasting ~ 20 minutes. The spectral range contains prominent quasar emission lines, encompassing both high- and low-ionization lines such as Lyα λ1216, Si IV λ1397, C IV λ1549, and C III] λ1909. Data reduction was carried out using standard IRAF routines for 2D long-slit spectroscopic data, including bias subtraction, flat-field and illumination correction, cosmic ray removal, wavelength calibration, background subtraction, extraction of 1D spectra, and stacking of the individual spectra from the nine exposures. Figure 1 presents the extracted spectra of the lensed images, while Figure 2 shows an image of the wide-separation lensed quasar SDSS J1326+4806.

In this study, we focus on the effects of microlensing on the broad wings of the high-ionization line C IV, as it is the most prominent feature within the observed wavelength range. First, we remove the continuum emission around the C IV line for each image by fitting a straight line to the adjacent continuum regions, carefully avoiding any known emission features. The line cores, produced by material spread over a wide region (including the narrow-line region and the outer parts of the broad-line region), are generally less affected by microlensing, as noted by [3] (but see [12] for an alternative view). Therefore, we use the line cores as a reference and establish a baseline little affected by microlensing by normalizing the emission line cores of images A and B. This normalization is achieved by defining the flux within a narrow interval around the line peak and scaling the spectrum of image B to match the core flux of image A. This procedure also removes the effects of macro-magnification and differential extinction (see, e.g., [9]). We then estimate the microlensing in the C IV line wings as $\mu_{\rm wing} = (m_A - m_B)_{\rm wing} - (m_A - m_B)_{\rm core}$, using a velocity range of 3000–10000 km s^{-1} on either side of the emission line peak. The velocity ranges are indicated in Figure 3, where we present the C IV line profile for both lensed images.

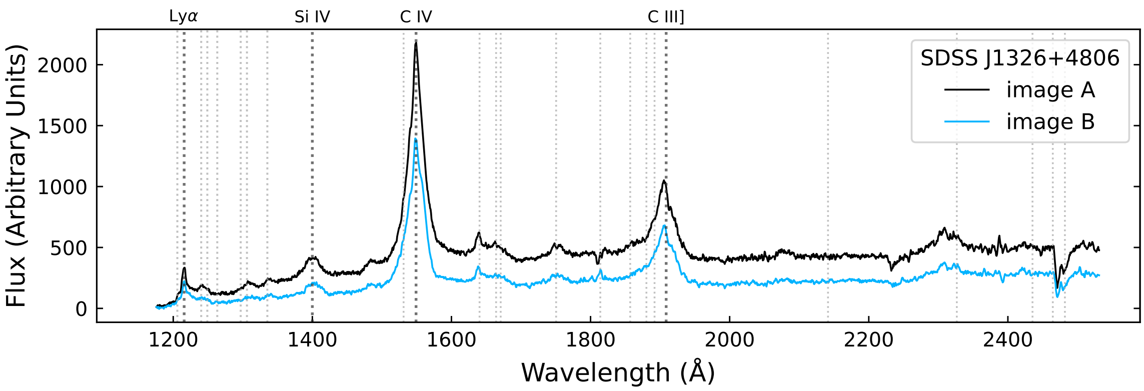

Figure 1: GTC spectra of SDSS J1326+4806, with image A shown in black and image B in blue. Thick vertical dotted lines mark prominent broad emission lines (Lyα, Si IV, C IV, and C III]), while gray vertical dotted lines indicate other emission features.

3 Methods

To simulate the microlensing effects of extended sources, we utilized the Fast Multipole Method – Inverse Polygon Mapping (FMM-IPM) algorithm ([14]). This method combines the FMM algorithm from [8] for calculating ray deflections with the IPM algorithm from [15, 17] for generating microlensing magnification maps. Our simulations cover a 3000×3000 pixel^2 area, which spans 100×100 R_E^2 on the source plane, where R_E represents the Einstein radius. For SDSS J1326+4806, the value of the Einstein radius is $R_E = 2.39 \times 10^{16}$cm $= 9.2$ light-days at the source plane assuming a mean microlens mass of $\langle m \rangle = 0.3 M_\odot$. The magnification maps have a high resolution of 0.31 light-days per pixel, effectively sampling the quasar's optical emission regions. These maps are defined by two key parameters: the local shear, γ, and the local convergence, κ, where κ is directly proportional to the surface mass density. These parameters were obtained by fitting a Singular Isothermal Sphere with external shear (SIS+γ_e) to the quasar images' positions. The local convergence is composed of two distinct components: $\kappa = \kappa_c + \kappa_\star$, where κ_c denotes the convergence attributed to continuously distributed matter, such as smooth dark matter, while $\kappa_\star$ corresponds to the convergence caused by stellar-mass point lenses, like microlens stars. The value of $\alpha \equiv \kappa_\star / \kappa$ represents the fraction of mass in compact objects and quantifies the contribution of stars to the total mass in the lens galaxy cluster. Since image B is situated far from the galaxies in the cluster, stellar microlensing is negligible, and we set α_B to zero. For image A, we varied α_A between 1% and 21%.

To model the structure of the unresolved quasar, we use circular Gaussian profiles ($I(R) \propto \exp(-R^2/2r_s^2)$) to simulate the luminosity distribution of the C IV emitting region. To calculate the magnifications for a source of size r_s, we convolve the magnification maps with Gaussian profiles having a sigma of r_s. It is widely accepted in the field that the specific shape of the source's emission profile has minimal impact on microlensing flux variability studies, as shown by [18] (although see [5]). The results are primarily determined by the half-light

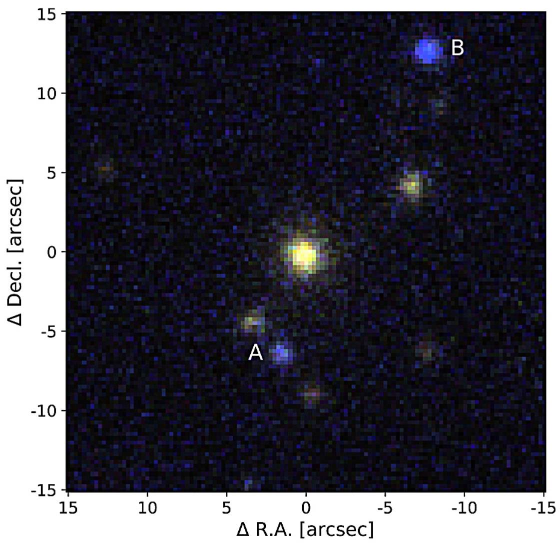

Figure 2: Pan-STARRS imaging data of the gravitationally lensed quasar SDSS J1326+4806. The two components are separated by 21″.06, with image A being located close (∼ 2″.7 and 3″.3) to two galaxies in the lens cluster. The field of view is approximately 0.25 square arcminutes.

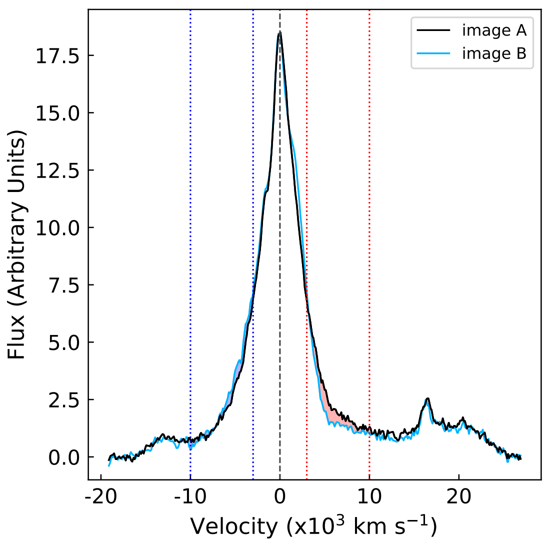

Figure 3: C IV line profiles of images A (black) and B (blue) after continuum subtraction and normalization of the line cores. The blue and red shaded regions highlight the windows selected for magnitude difference calculations. Observations reveal differences between the images in the red line wing.

radius rather than the detailed intensity profile. Many studies have used Gaussian intensity profiles to model the broad-line region in microlensing studies of quasars (see [19, 9, 3, 4]). These profiles are preferred due to their simplicity and effectiveness when convolved with magnification maps. As a result, we perform convolutions of the maps with Gaussians of different sizes of r_s, ranging from 1 to 30 light-days. The characteristic size r_s is related to the half-light radius by $R_{1/2} = 1.18 r_s$ for Gaussian profiles. After the convolution process, we normalize each magnification map by dividing it by its average value. The resulting histograms of these normalized maps depict the expected microlensing variability for various r_s values. Our strategy is to compare the observed microlensing magnification for a given image pair, $\mu_{\rm wing}$, with a statistical sample of simulated values for that measurement as a function of the source size (r_s) and the fraction of surface mass density in stars (α_A). This approach allows us to calculate the likelihood of the parameters (r_s, α_A) given the observations, $L(r_s, \alpha_A \mid \mu_{\rm wing})$ (for more details, see [13]).

4 Results and Discussion

We used Bayesian methods to estimate the probability of r_s based on the observed differential microlensing between images A and B in the wings of the C IV emission line. We measured microlensing magnifications of -0.21 mag in the red line wing and $+0.06$ mag in the blue

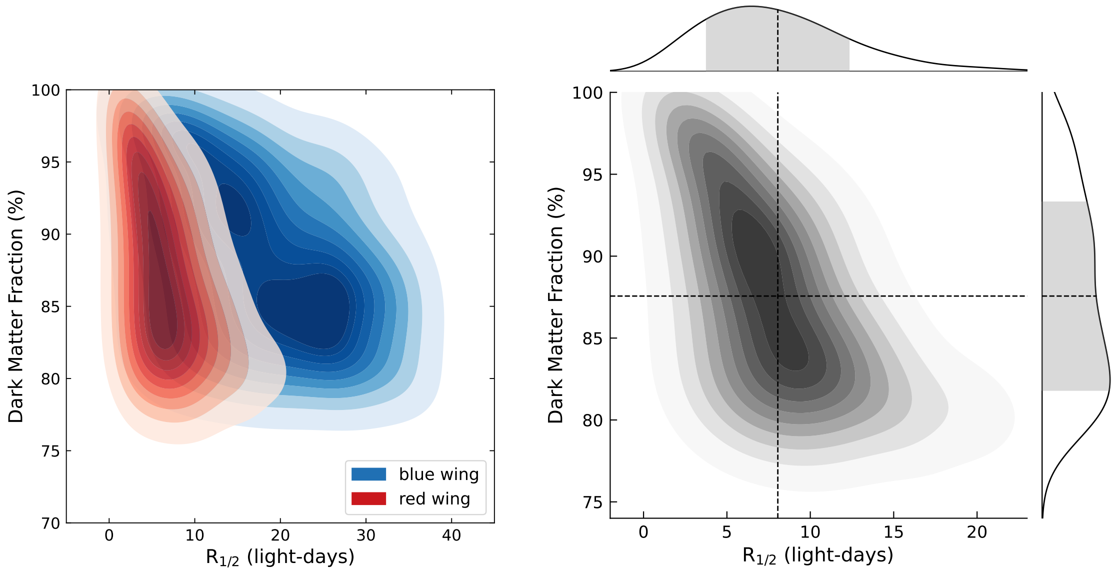

Figure 4: 2D kernel density estimation illustrating the probability distribution as a function of the size (x-axis) and the mass fraction (y-axis). The left panel displays separate analyses of the blue and red wings of the C IV emission line, while the right panel shows the combined probability distribution, obtained by multiplying the individual wing probabilities. Additionally, the right panel includes marginal probability distributions for both the smooth dark matter fraction and the C IV emitting region size along their respective axes.

wing, respectively. We inferred that the half-light radius of the C IV emitting region is $R_{1/2} = 8.1 \pm 4.3$ light-days, consistent with recent C IV emitting region size estimates of other gravitationally lensed quasars (see [6, 7]). Our Bayesian estimate for the mass fraction in stars is $12.4 \pm 5.7\%$ (at 68% confidence level), which is slightly smaller than the mass fraction in stars found based on microlensing measurements of 27 quasar image pairs seen through 19 lens galaxies ($\alpha = 0.21 \pm 0.14$, see [13]). The observed microlensing effects are likely caused by stars in the two galaxies nearest to image A within the lens cluster, located at distances of approximately 38 kpc and 46 kpc. Figure 4 shows the two-dimensional kernel density estimation illustrating the probability distribution as a function of the emitting region size and the smooth dark matter fraction. The left panel displays a separate analysis for the blue and red wings of the emission line, while the right panel shows the combined result from both wings, obtained by multiplying their respective probability distributions.

5 Conclusions

In this study, we explored the stellar-to-smooth dark matter fraction within the intracluster medium by examining microlensing effects in spectra obtained with the GTC of the wide-separation lensed quasar SDSS J1326+4806. Through analysis of the C IV emission line wings, we detected microlensing magnifications of up to approximately -0.2 mag. These microlensing effects are likely caused by stars within nearby galaxies, situated at distances on the order of tens of kiloparsecs from image A. However, compact dark matter objects such as primordial black holes might also be contributing to the observed effects, presenting an alternative explanation for the origin of microlensing ([10, 11]). We applied Bayesian methods to estimate the size of the C IV emitting region and the fraction of stellar-to-smooth dark matter in the vicinity image A. Our findings suggest that the half-light radius of the C IV emitting region is $R_{1/2} = 8.1 \pm 4.3$ light-days, consistent with recent size estimates in other systems ([6, 7]). Additionally, the stellar mass fraction near image A is $12.4 \pm 5.7\%$, which is lower than the stellar mass fraction obtained for lens galaxies ([13]). This work serves as a pilot study in a larger effort to explore microlensing in galaxy-cluster lensed quasars. Moving forward, we plan to extend this analysis to additional spectra obtained from the GTC for other quasar systems lensed by galaxy clusters. These future studies will further enhance our understanding of the mass composition within intracluster media.

References

[1] Fian, C., Mediavilla, E., Hanslmeier, A., et al. 2016, ApJ, 830, 149.

[2] Fian, C., Mediavilla, E., Jiménez-Vicente, J., et al. 2018, ApJ, 869, 132.

[3] Fian, C., Guerras, E., Mediavilla, E., et al. 2018, ApJ, 859, 50.

[4] Fian, C., Mediavilla, E., Motta, V., et al. 2021, A&A, 653, A109.

[5] Fian, C., Chelouche, D., & Kaspi, S. 2023, A&A, 677, A94.

[6] Fian, C., Jiménez-Vicente, J., Mediavilla, E., et al. 2024, ApJL, 972, L7.

[7] Fian, C., Muñoz, J. A., Jiménez-Vicente, J., et al. 2024, A&A, 689, A129.

[8] Greengard, L. & Rokhlin, V. 1987, Journal of Computational Physics, 73, 325.

[9] Guerras, E., Mediavilla, E., Jimenez-Vicente, J., et al. 2013, ApJ, 764, 160.

[10] Hawkins, M. R. S. 2022, MNRAS, 512, 5706.

[11] Hawkins, M. R. S. 2024, MNRAS, 527, 2393.

[12] Heydenreich, S., Mediavilla, E., Jiménez-Vicente, J., et al. 2024, arXiv:2409.04534.

[13] Jiménez-Vicente, J., Mediavilla, E., Kochanek, C. S., et al. 2015, ApJ, 799, 149.

[14] Jiménez-Vicente, J. & Mediavilla, E. 2022, ApJ, 941, 80.

[15] Mediavilla, E., Muñoz, J. A., Lopez, P., et al. 2006, ApJ, 653, 942.

[16] Mediavilla, E., Muñoz, J. A., Falco, E., et al. 2009, ApJ, 706, 1451.

[17] Mediavilla, E., Mediavilla, T., Muñoz, J. A., et al. 2011, ApJ, 741, 42.

[18] Mortonson, M. J., Schechter, P. L., & Wambsganss, J. 2005, ApJ, 628, 594.

[19] Motta, V., Mediavilla, E., Rojas, K., et al. 2017, ApJ, 835, 132.

[20] Schechter, P. L. & Wambsganss, J. 2004, Dark Matter in Galaxies, 220, 103.

[21] Shu, Y., Koposov, S. E., Evans, N. W., et al. 2019, MNRAS, 489, 4741.

[22] Wambsganss, J. 2006, Saas-Fee Advanced Course 33: Gravitational Lensing: Strong, Weak and Micro, 453